Journal of Solid State Chemistry **148,** 499–507 (1999)
Article ID jssc.1999.8487, available online at http://www.idealibrary.com on IDEAL®

Factors Influencing the Stabilization of Ni^+ in Perovskite-Related Oxides

A. Manthiram,[1] J. P. Tang, and V. Manivannan

Texas Materials Institute, The University of Texas at Austin, ETC 9.104, Austin, Texas 78712

Received February 3, 1999; in revised form July 28, 1999; accepted August 27, 1999

With an objective to identify the factors influencing the stabilization of the unusual valence state Ni^+ in perovskite-related oxides, the reduction of the Ruddlesden–Popper series precursors $A_{n+1}Ni_nO_{3n+1}$ (A = lanthanide and alkaline earth and $n = 1$, 2, and 3) containing the $Ni^{2+/3+}$ or $Ni^{3+/4+}$ couple has been investigated systematically. $La_{2-x}Sr_xNiO_{3+\delta}$, $Ln_3Ni_2O_{6+\delta}$ (Ln = lanthanide), and $Ln_4Ni_3O_8$ oxides containing the $Ni^{+/2+}$ couple have been obtained by a reduction of, respectively, $La_{2-x}Sr_xNiO_4$, $Ln_3Ni_2O_7$, and $Ln_4Ni_3O_{10}$ with dilute hydrogen over a narrow range of temperature. During the reduction process, oxygen atoms are removed from the NiO_2 planes of $La_{2-x}Sr_xNiO_4$ to give orthorhombic $La_{2-x}Sr_xNiO_{3+\delta}$, but from the rock salt planes present in between the NiO_2 planes of $Ln_3Ni_2O_7$ and $Ln_4Ni_3O_{10}$ to give tetragonal $Ln_3Ni_2O_{6+\delta}$ and $Ln_4Ni_3O_8$, respectively. Bond length matching between the stretched Ni^+–O and A–O bonds to minimize the internal stresses and coordination preference and size of the A cations are found to play an important role in accessing Ni^+. Although the $Ni^{+/2+}$ couple is isoelectronic with the $Cu^{2+/3+}$ couple in copper oxide superconductors, the $Ni^{+/2+}$ oxides exhibit localized semiconducting properties due to a larger charge transfer gap. © 1999 Academic Press

1. INTRODUCTION

The occurrence of high-temperature superconductivity in copper oxides (1) has stimulated interest in the investigation of other perovskite-related transition metal oxides. Nickel oxides belonging to the Ruddlesden–Popper (2) series $A_{n+1}Ni_nO_{3n+1}$ (A = lanthanide or alkaline earth and $n = 1, 2, 3,$ and ∞) have drawn much attention in this regard as Ni lies close to Cu in the periodic table and the Ni–O bond is sufficiently covalent (3–15). However, the nickel oxides with the $Ni^{2+/3+}$ couple exhibit a semiconductor to metal transition with doping rather than a semiconductor to superconductor transition. Although the $Ni^{2+/3+}$ couple is expected to have a small charge transfer gap Δ like the $Cu^{2+/3+}$ couple, the two couples differ in an important way. The $Cu^{2+/3+}$ couple with a $3d^{9-x}$ configuration and a larger site c/a ratio (ratio of Cu–O bond lengths along the z axis and in the xy plane, $(Cu–O)_z/(Cu–O)_{xy}$) (16) involves a completely filled d_{z^2} and partially filled $d_{x^2-y^2}$ bands. On the other hand, the $Ni^{2+/3+}$ couple with a d^{8-x} configuration and a smaller $(Ni–O)_z/(Ni–O)_{xy}$ ratio (17) involves both the partially filled d_{z^2} and $d_{x^2-y^2}$ bands. The holes are thus located only in the $d_{x^2-y^2}$ band in the copper oxide whereas they are located either in the d_{z^2} band or in both the d_{z^2} and $d_{x^2-y^2}$ bands, depending on the composition of the nickel oxides. The differences in the location and distribution of holes lead to the differences in properties between the two systems.

The differences in properties between the $Ni^{2+/3+}$ and $Cu^{2+/3+}$ couples have created interest in the investigation of the $Ni^{+/2+}$ couple, which is isoelectronic with the $Cu^{2+/3+}$ couple. However, the Ni^+:$3d^9$ energy in oxides is close to the Ni:4s energy and it is difficult to access Ni^+ in oxides by conventional high-temperature procedures. Reduction with hydrogen of appropriate oxide precursors at lower temperatures has become a feasible way to access Ni^+ in oxides. The first effort in this direction was by Crespin *et al.* (18, 19) to obtain the infinite-layer compound $LaNiO_2$ by a controlled hydrogen reduction of the perovskite oxide $LaNiO_3$. Following this, Crespin *et al.* (20, 21) also obtained $La_{1.6}Sr_{0.4}NiO_{3.47}$ and $LaSrNiO_{3.1}$ by reducing with hydrogen the corresponding $La_{2-x}Sr_xNiO_4$ precursor. More recently, Lacorre (22) has obtained $Ln_4Ni_3O_8$ (Ln = La, Pr, and Nd) by reducing $Ln_4Ni_4O_{10}$, and James and Attfield (23, 24) have obtained $YSr_5Ni_3O_8$ and $CeSr_7Ni_4O_{11}$ by reducing, respectively, $YSr_5Ni_3O_{11}$ and $CeSr_7Ni_4O_{15}$.

However, the factors that control the stabilization of Ni^+ have not been identified. We present in this paper a systematic effort to stabilize the $Ni^{+/2+}$ couple by reducing higher valent, perovskite-related nickel oxide precursors with an objective to identify the factors that stabilize Ni^+. The reductions of the Ruddlesden–Popper series $La_{2-x}Sr_xNiO_4$ ($n = 1$ member), Ln_2NiO_4 (Ln = Nd and Gd, $n = 1$ member), $La_{3-x}Nd_xNi_3O_7$ ($n = 2$ member), and

[1]To whom correspondence should be addressed. E-mail: rmanth@mail.utexas.edu.

0022-4596/99 $30.00

$La_{4-x}Nd_xNi_4O_{10}$ ($n = 3$ member) are investigated. The results demonstrate the importance of bond length matching between the adjacent layers as well as the coordination preferences of Ln^{3+} ions in stabilizing Ni^{+}.

2. EXPERIMENTAL

$La_{2-x}Sr_xNiO_4$ samples were synthesized by a coprecipitation method followed by firing at higher temperatures (7, 17). The coprecipitate obtained by adding equal amounts of KOH and K_2CO_3 to a dilute nitric acid solution consisting of required amounts of La_2O_3, $SrCO_3$, and $Ni(CH_3COO)_2 \cdot 4H_2O$ until the pH was about 13 was fired for 1–3 days either in air at 1000–1100°C for $x < 0.8$ or in a flowing oxygen atmosphere at 1100–1300°C for $x > 0.8$ to obtain $La_{2-x}Sr_xNiO_4$ for $0 \le x \le 1.5$. Other Ln_2NiO_4 (Ln = Nd and Gd) and $La_{4-x}Nd_xNi_3O_{10}$ ($0 \le x \le 4$) were obtained by a similar coprecipitation method and firing at, respectively, 1050°C in air for 1–2 days and 950–1100°C in an oxygen atmosphere for 3–5 days; the firing temperature had to be lowered with increasing x in $La_{4-x}Nd_xNi_3O_{10}$ from 1100°C for $x = 0$ to 950°C for $x = 4$ to stabilize the phases. $La_{3-x}Nd_xNi_2O_7$ ($0 \le x \le 1$) were obtained by the Pechini process (25) in which the gel obtained by adding citric acid and ethylene glycol to a dilute nitric acid solution of Ln_2O_3 and $Ni(CH_3COO)_2 \cdot 4H_2O$ was fired at 1150–1200°C in an oxygen atmosphere for 2–5 days. The precursor oxides so formed were characterized by X-ray powder diffraction and iodometric titration (26) to determine the oxygen contents.

The reduction of the higher valent nickel oxide precursors was carried out in a Perkin-Elmer Series 7 thermogravimetric analyzer (TGA) with a heating rate of 2°C/min in a flowing mixture of approximately 3% H_2, 30% Ar, and 67% N_2. Reduction experiments were also carried out in a tubular furnace at specific temperatures for 1–10 h in a mixture of 10% H_2 and 90% Ar. The products obtained after the reduction experiments were characterized by X-ray powder diffraction.

3. RESULTS AND DISCUSSION

3.1. Reduction of $La_{2-x}Sr_xNiO_4$

The $La_{2-x}Sr_xNiO_4$ samples have the T structure of K_2NiF_4 (Fig. 1a) and belong to the $n = 1$ member of the Ruddlesden–Popper series (2). Both the oxygen content and the oxidation state of nickel in the precursor $La_{2-x}Sr_xNiO_4$ before reduction are given in Table 1. While the sample with $x = 0$ has about 0.14 excess oxygen, the samples with $0.25 \le x \le 1.0$ are nearly stoichiometric, with oxygen contents close to 4.0, and those with $x > 1$ tend to have oxygen vacancies (17).

Figures 2 and 3 give the TGA plots of $La_{2-x}Sr_xNiO_4$ for various x values. The samples with $x < 1.0$ begin to lose oxygen above 200°C and give a plateau around 400°C corresponding to the stabilization of Ni^{2+}. The oxidation state of Ni at the beginning of the plateau corresponding to the point marked A in Fig. 2 is given in Table 1 and plotted in Fig. 4. X-ray diffraction analysis of the products obtained

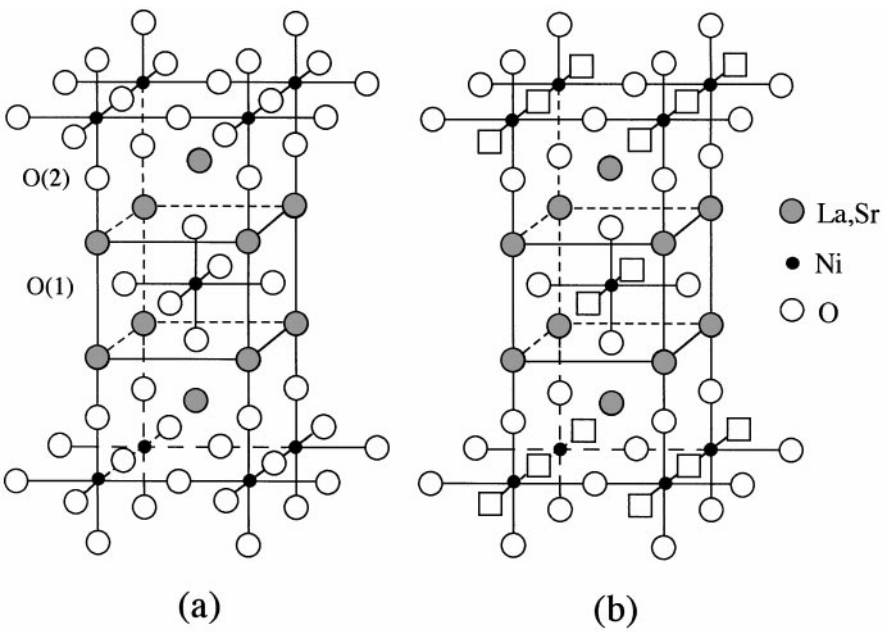

FIG. 1. Crystal structures of (a) tetragonal $La_{2-x}Sr_xNiO_4$ and (b) ideal, orthorhombic $La_{2-x}Sr_xNiO_3$.

TABLE 1
Compositional and Crystal Chemical Characterization of $La_{2-x}Sr_xNiO_4$ before and after Reduction

	Before reduction		After reduction[a]					
						Lattice parameters (Å)		
x	Oxygen content	Ni oxidation state	Oxygen content	Ni oxidation state	Structure type	a	b	c
0.0	4.14	2.28	3.97	1.94	T (ortho)	5.467(1)	5.532(1)	12.55(1)
0.25	4.03	2.31	3.88	2.01	T (tetra)	3.833(1)		12.50(1)
0.5	3.99	2.48	3.75	2.00	Sr_2CuO_3	3.799(3)	3.863(3)	12.65(1)
0.75	3.98	2.71	3.60	1.95	Sr_2CuO_3	3.752(1)	3.843(1)	12.70(1)
1.0	3.97	2.94	3.45	1.90	Sr_2CuO_3	3.726(1)	3.880(1)	12.68(1)
1.1	3.96	3.02	3.36	1.82	Sr_2CuO_3	3.726(2)	3.850(1)	12.65(1)
1.2	3.94	3.08	3.25	1.70	Sr_2CuO_3	3.686(1)	3.847(1)	12.64(1)
1.3	3.94	3.18	3.19	1.68	Sr_2CuO_3	3.636(1)	3.847(1)	12.64(1)
1.4	3.93	3.26	3.11	1.62	Sr_2CuO_3	3.639(1)	3.843(1)	12.63(1)
1.5	3.98	3.46	3.03	1.56	Sr_2CuO_3	3.559(1)	3.860(1)	12.64(1)

[a]After reduction to the point marked A in Figs. 2 and 3.

after heating the $La_{2-x}Sr_xNiO_4$ samples to point A in the TGA and cooling to room temperature is also given in Table 1. The sample with $x = 0$ has the orthorhombic T structure and that with $x = 0.25$ has the tetragonal T structure. On the other hand, the $La_{2-x}Sr_xNiO_{3+\delta}$ samples with $0.5 \leq x \leq 1.0$ have the orthorhombic Sr_2CuO_3-type structure (27). The ideal $La_{2-x}Sr_xNiO_3$ structure is shown in Fig. 1b in which the oxygen vacancies are ordered along the a axis of the K_2NiF_4 structure. The structure consists of double (La, Sr)O–(La, Sr)O rock salt layers alternating with a single NiO chain along the c axis. The $La_{2-x}Sr_xNiO_{3+\delta}$ samples formed in this study have the excess δ oxygen atoms present along the a axis. Above around 500–600°C, the $x \leq 1.0$ samples begin to lose oxygen rapidly, corresponding to the reduction of Ni^{2+} to metallic Ni. Thus the samples with $x \leq 1.0$ do not show a tendency to stabilize Ni^+. Attempts to stabilize Ni^+ by altering the hydrogen content in the reducing atmosphere were unsuccessful.

On the other hand, samples with $1.1 \leq x \leq 1.5$ begin to lose oxygen above about 300°C and do not exhibit a plateau above 400°C, corresponding to the stabilization of Ni^{2+}. Instead, a slow but steady loss of oxygen occurs beyond point A in a continuous manner after the initial rapid loss in oxygen. Point A corresponds to the temperature where La_2O_3 impurity begins to form. The oxidation state of Ni at point A for $x > 1$ is less than $2+$ and it decreases with increasing x (Table 1 and Fig. 4). X-ray diffraction analysis of the products obtained after heating the $La_{2-x}Sr_xNiO_4$ samples to point A in the TGA and cooling to room temperature indicates them to have the Sr_2CuO_3 structure, and the lattice parameters are given in Table 1 and plotted in Fig. 5. The decreasing a parameter with increasing x is due to a decreasing oxygen content on the a axis. Unlike for the $x < 1$ samples, the Sr_2CuO_3 structure was found to be maintained even after heating beyond point A up to about 600°C for the $x > 1$ samples, but the amount of La_2O_3 impurity increased to about 15–20%. These results clearly show that Ni^+ is stabilized in $La_{2-x}Sr_xNiO_4$ for $1 \leq x \leq 1.5$. The results also indicate that a continuous pathway from the K_2NiF_4-type structure to the oxygen-deficient Sr_2CuO_3-type structure exists in the $La_{2-x}Sr_xNiO_4$ system.

The stabilization of Ni^+ at higher concentrations of Sr^{2+} in $La_{2-x}Sr_xNiO_{3+\delta}$ can be understood by considering the bond length matching between the (La, Sr)–O and Ni–O bonds. Reduction of Ni^{n+} ions in $La_{2-x}Sr_xNiO_4$ to Ni^+ will result in an increase of the Ni–O bond length. At smaller Sr^{2+} concentrations, formation of Ni^+ will introduce a significant amount of compressive stress in the Ni–O bonds, which results in an inaccessibility of Ni^+ for $x < 1$ in $La_{2-x}Sr_xNiO_{3+\delta}$. At higher Sr^{2+} concentrations, an increased (La, Sr)–O bond length can lower the compressive stress in the Ni–O bonds by providing a better bond length matching and stabilize Ni^+ in $La_{2-x}Sr_xNiO_{3+\delta}$ for $x > 1$. A decreasing oxidation state of Ni below $2+$ at point A in Fig. 3 with increasing $x > 1$ is due to a better bond length matching provided by the increasing Sr content. This consideration is further supported by the fact that all Ni^+ could be stabilized by having a larger amount of Sr in $YSr_5Ni_3O_8$ (23) and $CeSr_7Ni_4O_{11}$ (24), both of which have the Sr_2CuO_3 structure with some oxygen vacancies. $YSr_5Ni_3O_8$ and $CeSr_7Ni_4O_{11}$ were obtained by reducing, respectively, the $x = 1.67$ member of $Y_{2-x}Sr_xNiO_{4-\delta}$ and the $x = 1.75$ member of $Ce_{2-x}Sr_xNiO_{4-\delta}$, both of which have the T structure of La_2NiO_4.

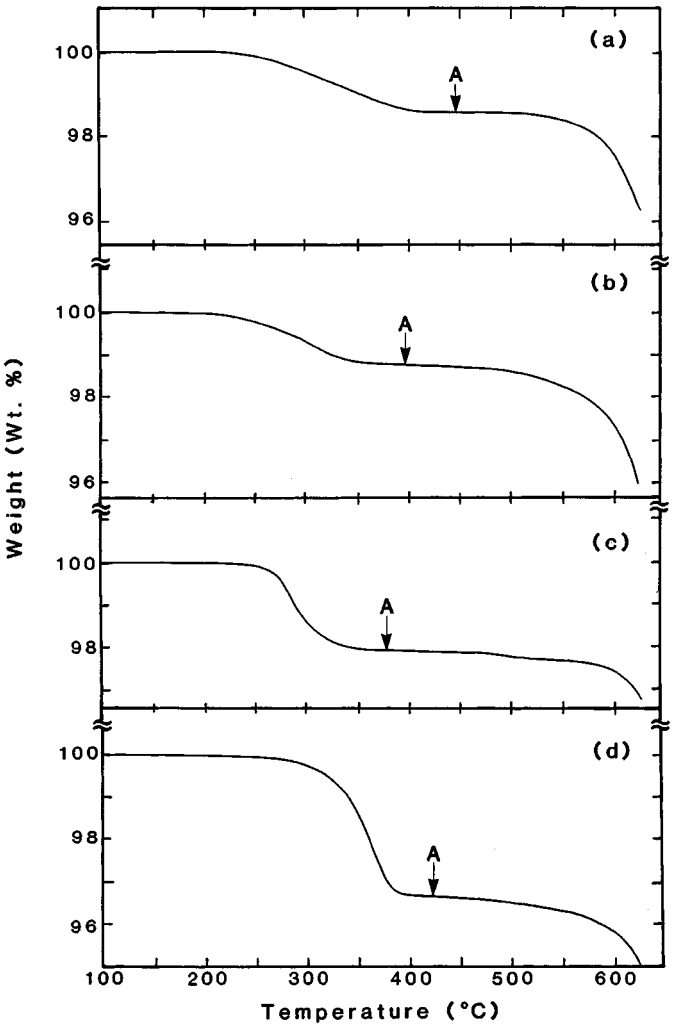

FIG. 2. TGA plots of $La_{2-x}Sr_xNiO_4$: (a) $x = 0$, (b) $x = 0.25$, (c) $x = 0.5$, and (d) $x = 0.75$.

Although our dynamic reduction process of the $La_{2-x}Sr_xNiO_4$ phases results in the formation of a small amount of La_2O_3 impurity for $x \geq 1$ and does not stabilize appreciable Ni^+ for $x < 1$, Crespin *et al.* (20, 21) have shown using a static reduction technique that single-phase $La_{1.6}Sr_{0.4}NiO_{3.47}$ and $LaSrNiO_{3.1}$ could be obtained by reducing the corresponding $La_{2-x}Sr_xNiO_4$ phases. The decreasing oxygen content and oxidation state of Ni with increasing x again illustrates the role of bond length matching in stabilizing Ni^+. The static reduction procedure of Crespin *et al.* (20, 21) employed a specially designed closed gas system in which the degree of reduction could be monitored by following the volume of hydrogen consumed. The differences in the oxidation state of Ni in the products obtained by dynamic and static reduction procedures reveal that the extent of stabilization of Ni^+ is sensitive to the synthesis conditions.

3.2. *Reduction of Ln_2NiO_4 (Ln = Nd and Gd)*

As the size of Ln^{3+} ions decreases in Ln_2CuO_4, the LnO–LnO double rock salt layers transform into a Ln_2O_2 fluorite layer to give the tetragonal T′ structure (28). For example, La_2CuO_4 has the T′ structure whereas other Ln_2CuO_4 for Ln = Pr, Nd, Sm, and Gd have the T′ structure. On the other hand, the Ln_2NiO_4 (Ln = Pr, Nd, Sm, and Gd) all have the T structure. One possibility to access T′ Ln_2NiO_4 is that a reduction of the Ln_2NiO_4 oxides with smaller Ln^{3+} ions may increase the Ni–O bond length and force the rock salt layers to transform to the fluorite arrangement to provide a better bond length matching for the stretched Ni–O bonds. For a given Ln^{3+} ion, the fluorite arrangement will be more stretched in the xy plane than the rock salt arrangement due to a direct electrostatic repulsion

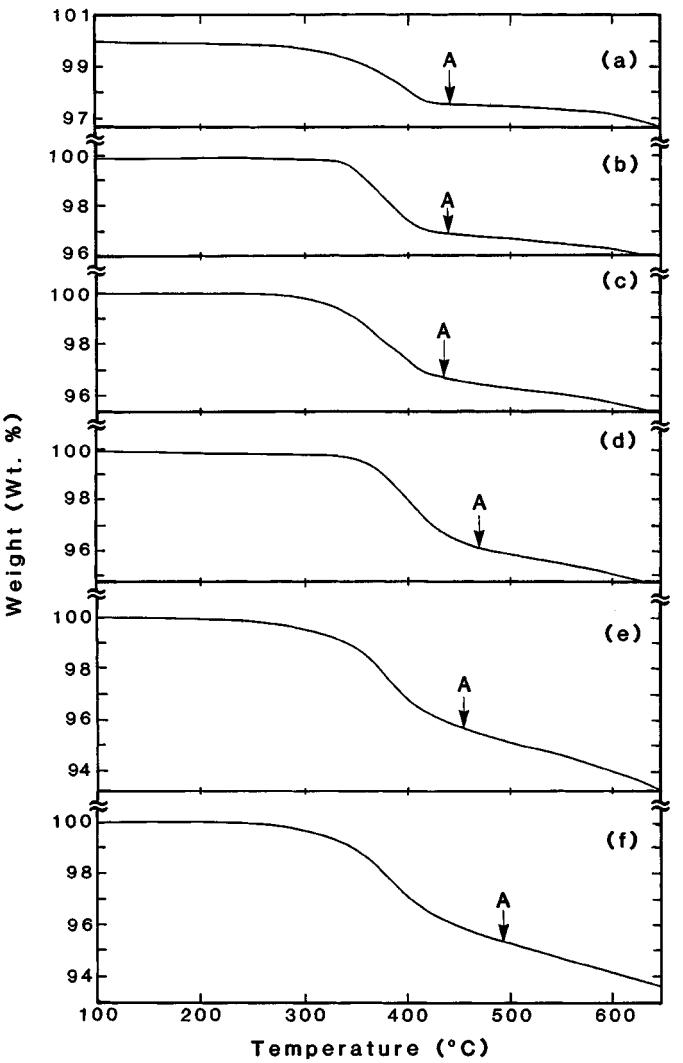

FIG. 3. TGA plots of $La_{2-x}Sr_xNiO_4$: (a) $x = 1.0$, (b) $x = 1.1$, (c) $x = 1.2$, (d) $x = 1.3$, (e) $x = 1.4$, and (f) $x = 1.5$.

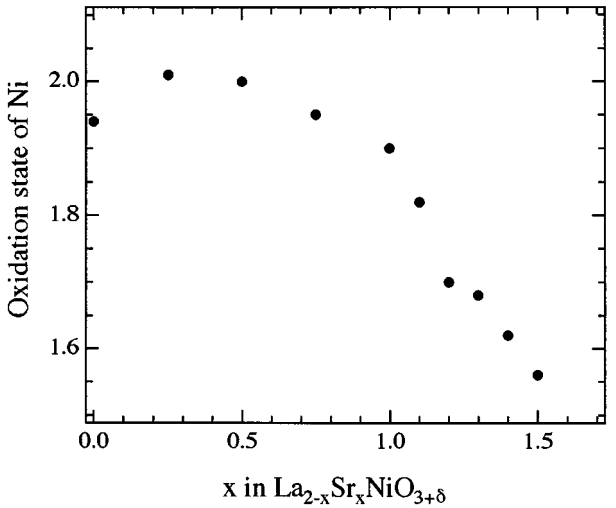

FIG. 4. Variation with x of the oxidation state of Ni at the point marked A in Figs. 2 and 3.

between the oxide ions in the tetrahedral sites of the fluorite layer (29).

With this objective, we carried out the reduction of $Ln_2NiO_{4+\delta}$ for $Ln = Nd$ and Gd and the TGA plots are shown in Fig. 6. Both samples lose the excess δ oxygen above 200°C like $La_2NiO_{4+\delta}$ (Fig. 2a) and the plateau around 400°C corresponds to the stabilization of Ni^{2+}. Further increase in reduction temperature results in a drastic weight loss above 450°C and the formation of metallic Ni, suggesting that Ni^+ could not be accessed.

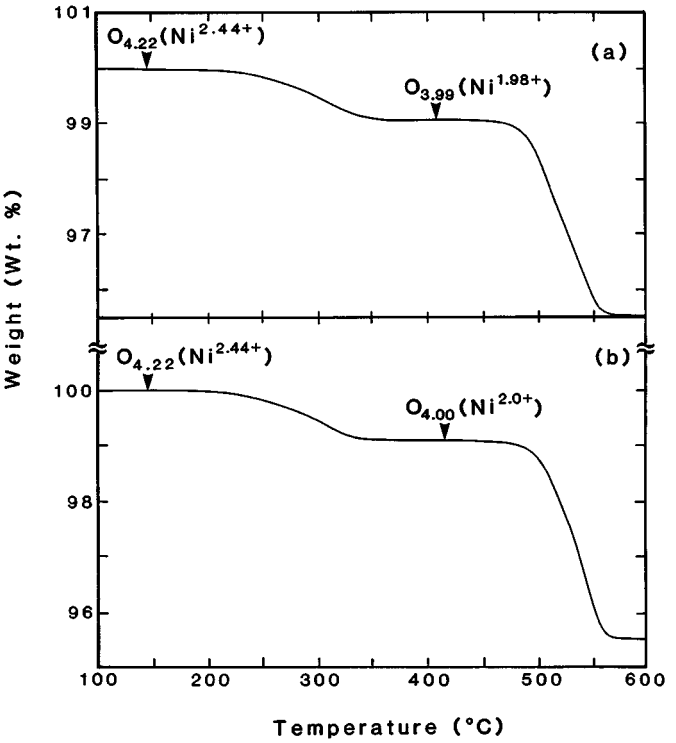

FIG. 6. TGA plots of (a) $Nd_2NiO_{4+\delta}$ and (b) $Gd_2NiO_{4+\delta}$.

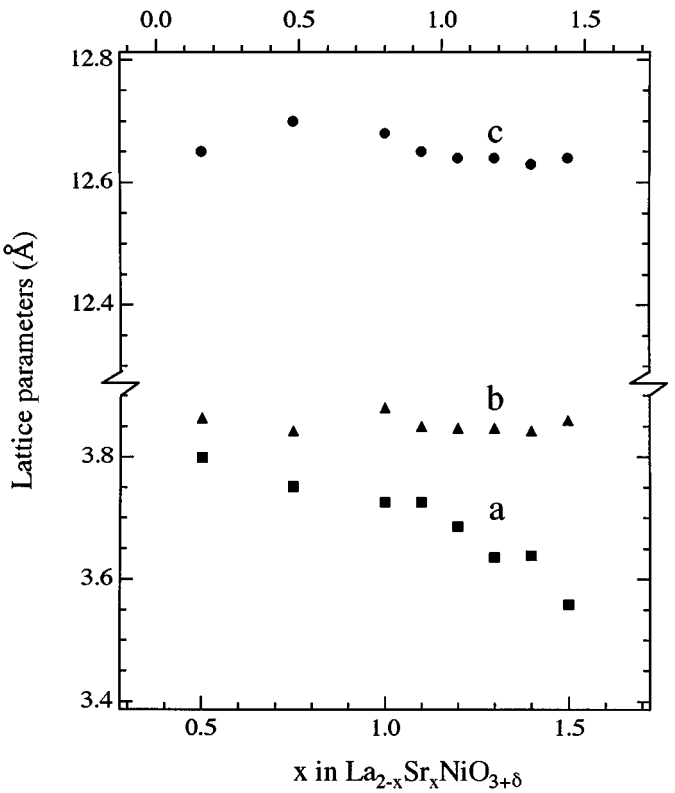

FIG. 5. Variation with x of the lattice parameters of the products $La_{2-x}Sr_xNiO_{3+\delta}$ that were obtained at point A in Figs. 2 and 3.

The X-ray diffraction patterns of the products obtained after reducing to 400°C (first plateau in Fig. 6) are compared with that recorded before the reduction in Fig. 7. Although the X-ray pattern after reduction appears similar to that expected for a T′ structure, lattice parameter refinements (Table 2) clearly show that the sample is still orthorhombic, belonging to the T structure. However, the degree of orthorhombicity has increased dramatically after reduction due to an increased internal stress and bond length mismatch. The orthorhombic distortion in the reduced sample is so high that the (020) reflection has moved significantly to lower angles and merged with the (113) reflection, which makes the X-ray pattern appear similar to that of a T′ structure. Thus the T′ structure could not be stabilized for Ln_2NiO_4.

3.3. *Reduction of $La_{3-x}Nd_xNi_2O_7$ ($0 \le x \le 1$)*

The $La_{3-x}Nd_xNi_2O_7$ phases belong to the $n = 2$ member of the Ruddlesden–Popper series and have the layer structure shown in Fig. 8a. The TGA plots of $La_{3-x}Nd_xNi_2O_{7-\delta}$ for $x = 0$ and 1 are shown in Fig. 9. Both samples, with an

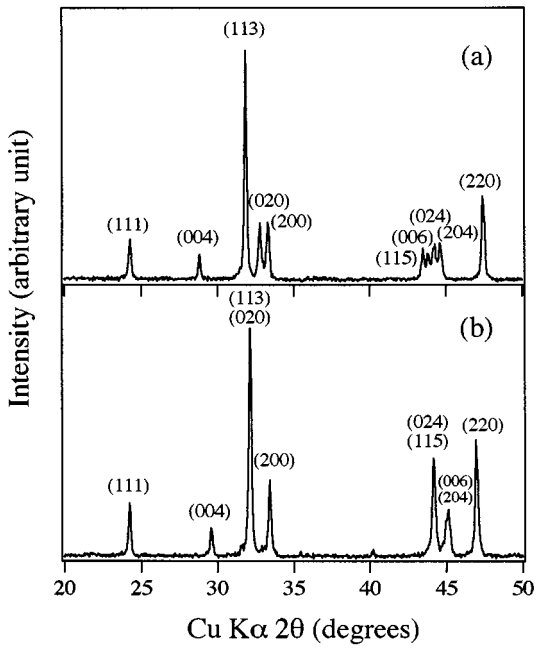

FIG. 7. X-ray diffraction patterns of Nd_2NiO_4: (a) before reduction and (b) after reduction to 400°C in the TGA balance.

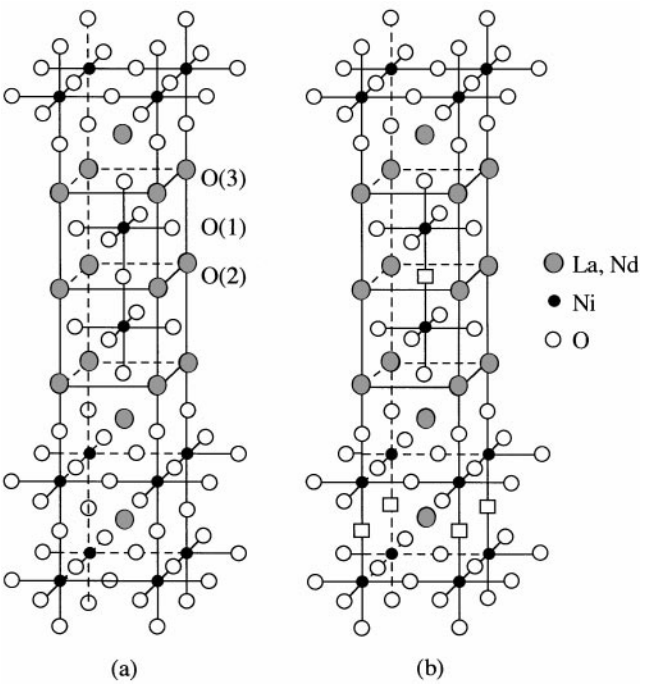

FIG. 8. Crystal structures of (a) $La_{3-x}Nd_xNi_2O_7$ and (b) $La_{3-x}Nd_xNi_2O_6$.

oxygen content close to 7 before reduction, begin to lose oxygen above 250°C and exhibit a plateau around 450°C. The oxygen content values before reduction and after reduction to about 450°C are indicated in the plots. The plateau around 450°C in Fig. 9 corresponds to the formation of an intermediate phase containing Ni^+. The intermediate phase in the $x = 0$ member has an oxygen content of 6.37 and a nickel oxidation state of 1.87+, which are in close agreement with those found by Zhang and Greenblatt (15). However, the reduction of $La_2NdNi_2O_7$ has not been investigated before. As we see, the intermediate phase in the $La_2NdNi_2O_7$ system has an oxygen content of 5.92 and a nickel oxidation state of 1.42+, which are significantly lower than that found in the reduction product of the $La_3Ni_2O_7$ system. The lattice parameters of the parent $Ln_3Ni_2O_7$ and the intermediate phases obtained around 450°C are compared in Table 3. A larger a parameter for $La_2NdNi_2O_{5.92}$ compared to that for $La_3Ni_2O_{6.37}$ is consistent with a larger Ni^+ concentration in the former.

TABLE 2
Comparison of the Lattice Parameters of Ln_2NiO_4 (Ln = La, Nd, and Gd) before and after Reduction

	Lattice parameters (Å)					
	Before reduction			After reduction[a]		
Sample	*a*	*b*	*c*	*a*	*b*	*c*
La_2NiO_4	3.859(1)		12.675(5)	5.467(1)	5.532(1)	12.552(9)
Nd_2NiO_4	5.365(1)	5.451(1)	12.355(4)	5.381(1)	5.584(1)	12.139(6)
Gd_2NiO_4	5.361(1)	5.443(1)	12.342(5)	5.383(1)	5.579(1)	12.134(6)

[a]After reduction to 400°C.

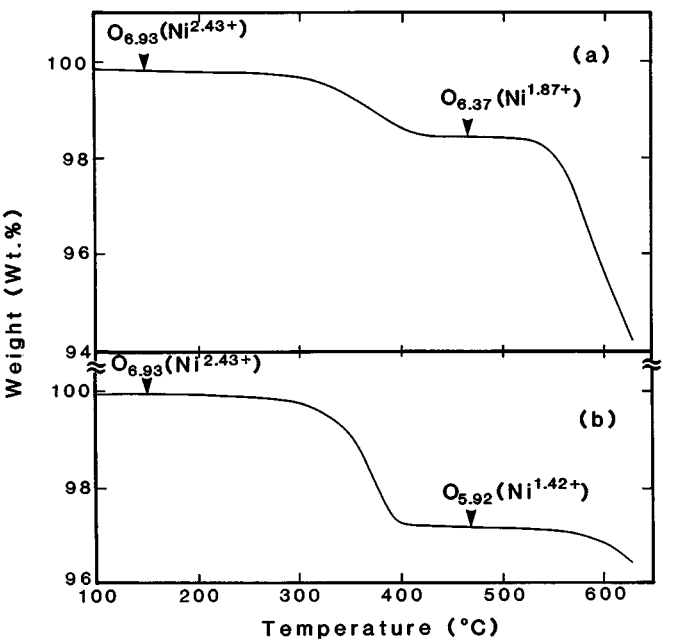

FIG. 9. TGA plots of (a) $La_3Ni_2O_7$ and (b) $La_2NdNi_2O_7$.

TABLE 3
Comparison of the Lattice Parameters of $Ln_{3-x}Nd_xNi_2O_7$ before and after Reduction

	Lattice parameters (Å)				
	Before reduction			After reduction[a]	
Sample	*a*	*b*	*c*	*a*	*c*
$La_3Ni_2O_7$	5.397(1)	5.445(1)	20.573(5)	3.879(1)	20.051(7)
$La_2NdNi_2O_7$	5.350(1)	5.448(1)	20.386(6)	3.946(1)	19.737(7)

[a]After reduction to 450°C.

During the reduction of the $Ln_3Ni_2O_7$ oxides, oxygen atoms are removed from the O(2) sites of the *Ln*O layers that are in between the two NiO_2 sheets (Fig. 8) as shown by Zhang and Greenblatt (15) during the reduction of $La_3Ni_2O_7$. We believe that our ability to achieve a lower oxygen content with a significantly lower nickel oxidation state in $La_2NdNi_2O_{5.92}$ is due to the ability of the smaller Nd^{3+} ions to adopt 8-fold oxygen coordination compared to the larger La^{3+} ions. It is possible that the La^{3+} ions may be present in the double rock salt layers (*Ln*(3) sites) and the Nd^{3+} ions may be present in between the two NiO_2 layers (*Ln*(2) sites) in $La_2NdNi_2O_{5.92}$ (Fig. 8b) so that the smaller Nd^{3+} ions can have 8-fold coordination and the larger La^{3+} ions can have 9-fold coordination. Future neutron diffraction studies can verify this prediction. The observed tetragonal symmetry for the reduced $Ln_{3-x}Nd_xNi_2O_{7-\delta}$ phases (Table 3) is consistent with the presence of oxygen vacancies in the O(2) sites. If the oxygen vacancies are present in the NiO_2 sheets (O(1) sites) as in the case of $La_{2-x}Sr_xNiO_{4-\delta}$ phases (see Section 3.1), then an orthorhombic symmetry may be expected.

3.4. Reduction of $La_{4-x}Nd_xNi_3O_{10}$ ($0 \le x \le 4.0$)

The $La_{4-x}Nd_xNi_3O_{10}$ phases belong to the $n = 3$ member of the Ruddlesden–Popper series and have the layer structure shown in Fig. 10a. The TGA plots of $La_{4-x}Nd_xNi_3O_{10}$ ($0 \le x \le 4.0$) are shown in Fig. 11. All the samples with an oxygen content close to 10 before reduction begin to lose oxygen above about 300°C. The $x = 0$ sample shows a plateau around 450°C corresponding to the formation of $La_4Ni_3O_9$ with all Ni^{2+}. The $x = 0$ sample then loses oxygen drastically above 500°C and leads to the formation of metallic Ni and La_2O_3 without exhibiting any plateau corresponding to the formation of the phase $La_4Ni_3O_8$. On the other hand, the samples with $2 \le x \le 4$ show a plateau around 480°C corresponding to the formation of $La_{4-x}Nd_xNi_3O_8$ with $Ni^{1.33+}$ without exhibiting any plateau corresponding to the formation of the phase $La_{4-x}Nd_xNi_3O_9$. The $x = 1$ sample is intermediate between the $x = 0$ and $2 \le x \le 4$ samples and it does not exhibit any well-defined plateau corresponding to the formation of the phases $La_3NdNi_3O_9$ or $La_3NdNi_3O_8$.

We have also investigated the reduction of the $Ln_{4-x}Nd_xNi_3O_{10}$ phases with a flowing gas mixture of 10% H_2 and 90% Ar in a tubular furnace at 230–360°C for about 1 h. X-ray diffraction analysis of the products obtained after the reduction experiments is given in Table 4. While both the O_9 and O_8 phases could be obtained for $0 \le x \le 2$, only the O_8 phase could be obtained without any indication for the formation of the O_9 phase for $x = 4$. The $x = 3$ sample also tends to form mostly the O_8 phase, with only a slight indication for the formation of the O_9 phase. It is clear from the data that the tendency to form the O_8 phase increases and that for the O_9 phase decreases with increasing x, which is consistent with the TGA data. However, the reduced phases are formed at a lower temperature in the tubular furnace experiments compared to the TGA experiments. This is due to the higher hydrogen content in the gas mixture and longer dwell time at a given temperature in the former case. Also, the access to the O_9 phases for $1 \le x \le 2$ and O_8 phase for $x = 0$ in the tubular furnace experiments

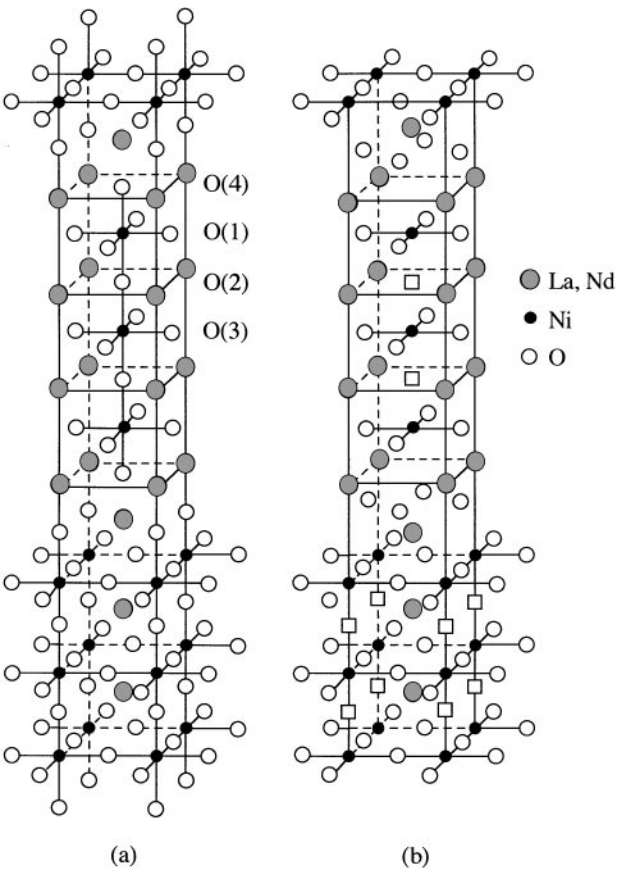

FIG. 10. Crystal structures of (a) $La_{4-x}Nd_xNi_3O_{10}$ and (b) $La_{4-x}Nd_xNi_3O_8$.

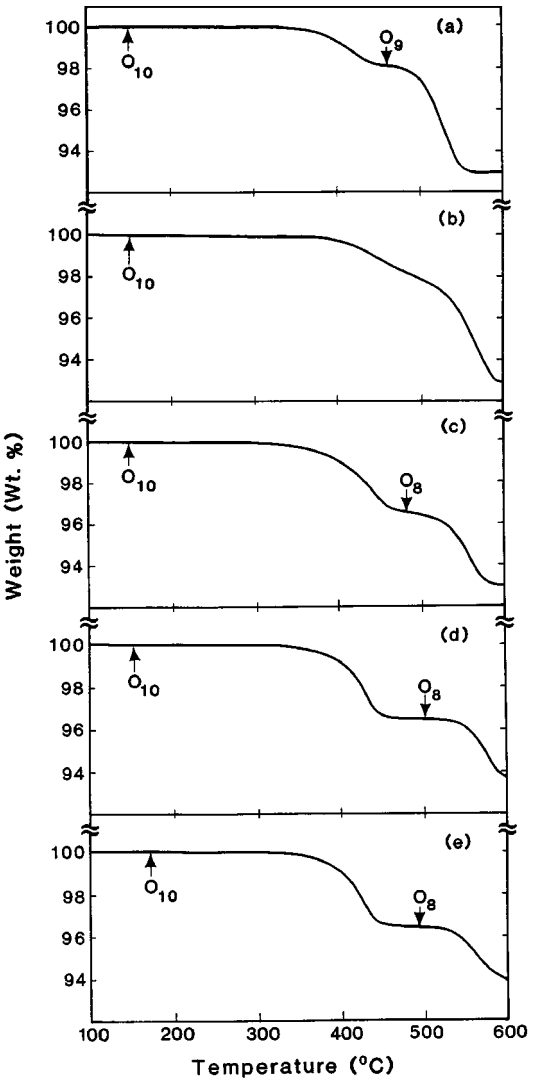

FIG. 11. TGA plots of $La_{4-x}Nd_xNi_3O_{10}$: (a) $x=0$, (b) $x=1$, (c) $x=2$, (d) $x=3$, and (e) $x=4$.

compared to the TGA experiments is due to the differences in the reaction conditions.

Lacorre (22) has shown that the oxygen atoms are removed from the O(2) sites of the *Ln*O layers that are located in between the NiO_2 layers (Fig. 10) during the formation of $Ln_4Ni_3O_8$ from $Ln_4Ni_3O_{10}$. Also, the double *Ln*O–*Ln*O rock salt layers rearrange to give a Ln_2O_2 fluorite arrangement in $Ln_4Ni_3O_8$. The $Ln_4Ni_3O_8$ oxides thus have a T′ structure with 4-fold square coordination for nickel and it is the only nickel oxide to date that has the T′ arrangement (Fig. 10b). We believe the transformation of the rock salt arrangement to the fluorite arrangement upon reducing the $Ln_4Ni_3O_{10}$ to $Ln_4Ni_3O_8$ is to provide a better bond length matching to the stretched Ni^+–O bonds. The fluorite arrangement will be stretched more in the *xy* plane than the rock salt arrangement due to a direct electrostatic repulsion between the oxide ions in the tetrahedral sites of the fluorite layer and, therefore, can lower the compressive stress in the longer Ni^+–O bonds.

We believe the easier formation of $Ln_4Ni_3O_8$ phases with increasing concentration of Nd is due to the ability of the smaller Nd^{3+} ions to adopt 8-fold coordination compared to the larger La^{3+} ions. The Ln^{3+} ions both in the fluorite layers and in between the NiO_2 layers in the T′ $La_{4-x}Nd_xNi_3O_8$ phases all have 8-fold coordination (Fig. 10b) and, therefore, a higher concentration of Nd^{3+} can favor the stabilization of the O_8 phase compared to the O_9 phase. Although the crystal structure of the O_9 phase could not be refined by Lacorre (22) due to the poor crystallinity, we believe that it may still maintain the rock salt arrangement like in the parent O_{10} phase. This is because with all Ni^{2+}, the *Ln*O–*Ln*O double rock salt arrangement can still provide a good bond length matching to the Ni^{2+}–O bonds in the O_9 phase. However, the substitution of a smaller Nd^{3+} for La^{3+} will increase the compressive stress in the Ni^{2+}–O bonds with a rock salt arrangement or introduce tensile stress in the Ni^{2+}–O bonds with a fluorite arrangement. Therefore, the stabilization of the O_9 phase becomes difficult with increasing concentration of Nd^{3+}. On the other hand, with a smaller Nd^{3+} and a fluorite arrangement, the tensile stress in the Ni^+–O bonds will be lower in the O_8 phase and, therefore, the formation of the O_8 phase becomes easier. The oxygen vacancies in the O_9 phase may be present in the O(2) sites in between the NiO_2 layers as in the case of $La_{3-x}Nd_xNi_2O_{7-\delta}$ phases (15), and not in the NiO_2 sheets, as indicated by the tetragonal symmetry (22).

3.5. *Electronic Properties*

As pointed out in Section 1, Ni^+:$3d^9$ is isoelectronic with Cu^{2+}:$3d^9$ and the mixed-valent $Ni^{+/2+}$ is analogous to the

TABLE 4
Comparison of the Relative Formation of $Ln_4Ni_3O_9$ and $Ln_4Ni_3O_8$ Phases on Reducing the $La_{4-x}Nd_xNi_3O_{10}$

Reduction temperature (°C)	Phase analysis[a]				
	$x=0$	$x=1$	$x=2$	$x=3$	$x=4$
235	O_{10}	O_{10}	O_{10}	O_{10}	$O_{10}+O_8$
255	O_{10}	$O_{10}+O_9$	O_{10}	$O_{10}+O_9$	$O_{10}+O_8$
280	$O_{10}+O_9$	O_9	$O_{10}+O_9$	O_9+O_8	O_8
295	$O_{10}+O_9$	O_9	O_9	O_9+O_8	O_8
305	$O_{10}+O_9$	O_9+O_8	O_9	O_8	O_8
315	O_9	O_8	O_9+O_8	O_8	O_8
335	O_9+O_8	O_8	O_8	O_8	O_8
355	O_8	O_8	O_8	O_8	O_8

[a] O_{10}, O_9, and O_8 refer, respectively, to the $Ln_4Ni_3O_{10}$, $Ln_4Ni_3O_9$, and $Ln_4Ni_3O_8$ phases.

p-type copper oxide superconductors. However, the $La_{2-x}Sr_xNiO_{3+\delta}$, $Ln_3Ni_2O_{6+\delta}$, and $Ln_4Ni_3O_8$ phases containing the $Ni^{+/2+}$ couple exhibit semiconducting behavior with a localized magnetic moment. For example, $La_4Ni_3O_8$ shows a localized magnetic moment with an antiferromagnetic ordering temperature of 40 K. $YSr_5Ni_3O_8$ has also been shown to be a semiconductor (23). The localized semiconducting properties of the $Ni^{+/2+}$ oxides are due to a much larger charge transfer energy Δ compared to that for the $Cu^{2+/3+}$ oxides. The $Ni^{+/2+}$ and $Ni^{2+/3+}$ oxides exhibit properties different from that of the copper oxides due to (i) more ionic $(NiO_2)^{(3-x)-}$ sheets in the former compared to the $(CuO_2)^{(2-x)-}$ sheets and (ii) the involvement of both the d_{z^2} and the $d_{x^2-y^2}$ bands in $Ni^{2+/3+}$ oxides (17) compared to a single $d_{x^2-y^2}$ band in $Cu^{2+/3+}$ oxides despite a comparable charge transfer gap.

4. CONCLUSIONS

Stabilization of the unusual valence Ni^{+} in perovskite-based intergrowth oxides has been investigated systematically by reducing the corresponding Ruddlesden–Popper series $A_{n+1}Ni_nO_{3n+1}$ ($n = 1$, 2, and 3) precursors containing the $Ni^{2+/3+}$ or $Ni^{3+/4+}$ couple. The Ni^{+} state is unstable in oxides and it could be accessed only by a reduction of the oxide precursors over a narrow range of temperature. The investigation reveals that the bond length matching between the stretched Ni^{+}–O and *A*–O bonds and the coordination preference of the *A* cations control the stabilization of Ni^{+}. Although T′ Ln_2CuO_4 are well known. T′ $Ln_2NiO_{4-\delta}$ could not be accessed. The T′ arrangement could be stabilized only for the $n = 3$ member ($Ln_4Ni_3O_8$) of the Ruddlesden–Popper series of the nickel oxides. While oxygen atoms are removed from the NiO_2 planes of the $n = 1$ member, they are removed from the rock salt layers present in between the NiO_2 planes of the $n = 2$ and 3 members. The $Ni^{2+/3+}$ oxides exhibit localized semiconducting properties due to a larger charge transfer gap.

Although the formation of the infinite-layer compound $LaNiO_2$ has been reported (i) by a reduction of the $LaNiO_3$ perovskite in a closed glass apparatus under static conditions (18, 19) and (ii) by a reduction in the TGA balance with hydrogen of $LaNiO_3$ that was synthesized in the presence of a significant amount of Na_2CO_3 flux (30), our attempts to stabilize $LaNiO_2$ either in the TGA experiments or in tubular furnace experiments were unsuccessful even when we synthesized $LaNiO_3$ in the presence of Na_2CO_3 flux. Changing the concentration of H_2 in the gas mixture also did not help. The reduction gives $La_2Ni_2O_5$ with all Ni^{2+} first and then La_2O_3 and Ni metal. It is clear that the control of the synthesis conditions is crucial in accessing the unusual valence state Ni^{+}.

ACKNOWLEDGMENT

Acknowledgment is made to the Welch Foundation (Grant F-1254) and the donors of the Petroleum Research Fund, administered by the American Chemical Society (Grant ACS-PRF 32410-AC5), for support of this research.

REFERENCES

1. J. G. Bednorz and K. A. Muller, *Z. Phys. B* **64,** 189 (1986).
2. S. N. Ruddlesden and P. Popper, *Acta Crystallogr.* **11,** 54 (1959).
3. Z. Kakol, J. Spalek, and J. M. Honig, *J. Solid State Chem.* **79,** 288 (1989).
4. K. Sreedhar and C. N. R. Rao, *Mater. Res. Bull.* **25,** 1235 (1990).
5. B. W. Arbuckle, K. V. Ramanujachary, Z. Zhang, and M. Greenblatt, *J. Solid State Chem.* **88,** 278 (1990).
6. Y. Takeda, R. Kanno, M. Sakano, O. Yamamoto, M. Takano, Y. Bando, H. Akinaga, K. Takita, and J. B. Goodenough, *Mater. Res. Bull.* **25,** 293 (1990).
7. C. J. Liu, M. D. Mays, D. O. Cowan, and M. G. Sanchez, *Chem. Mater.* **3,** 495 (1991).
8. R. J. Cava, B. Batlogg, T. T. Palstra, J. J. Krajewski, W. F. Peck, Jr., A. P. Ramirez, and L. W. Rupp, Jr., *Phys. Rev. B* **43,** 1229 (1991).
9. J. B. Torrance, P. Lacorre, A. I. Nazzal, E. J. Ansaldo, and C. Niedermayer, *Phys. Rev. B* **45,** 8209 (1992).
10. X. Granados, J. Fontcuberta, J. Alonso, M. Vallet-Regi, and J. M. Gonzalez-Calbert, *Physica C* **191,** 371 (1992).
11. X. Granados, J. Fontcuberta, M. Vallet-Regi, M. J. Sayagues, and J. M. Gonzalez-Calbert, *J. Solid State Chem.* **102,** 455 (1993).
12. K. Sreedhar and J. M. Honig, *J. Solid State Chem.* **111,** 147 (1994).
13. Z. Zhang, M. Greenblatt, and J. B. Goodenough, *J. Solid State Chem.* **108,** 402 (1994).
14. K. Sreedhar, M. McElfresh, D. Perry, D. Kim, P. Metcalf, and J. M. Honig, *J. Solid State Chem.* **110,** 208 (1994).
15. Z. Zhang and M. Greenblatt, *J. Solid State Chem.* **117,** 236 (1995).
16. M. Braden, P. Schweiss, G. Heger, W. Reichardt, Z. Fisk, K. Gamayunov, I. Tanaka, and H. Kojima, *Physica C* **223,** 396 (1994).
17. J. P. Tang, A. Manthiram, Q. Huang, and M. Crawford, to be submitted.
18. M. Crespin, P. Levitz, and L. Gatineau, *J. Chem. Soc., Faraday Trans. 2* **79,** 1181 (1983).
19. P. Levitz, M. Crespin, and L. Gatineau, *J. Chem. Soc., Faraday Trans. 2* **79,** 1195 (1983).
20. M. Crespin, J. M. Bassat, P. Odier, P. Mouron, and J. Choisnet, *J. Solid State Chem.* **84,** 165 (1990).
21. M. Crespin, C. Landron, P. Odier, J. M. Bassat, P. Mouron, and J. Choisnet, *J. Solid State Chem.* **100,** 281 (1992).
22. Ph. Lacorre, *J. Solid State Chem.* **97,** 495 (1992).
23. M. James and J. P. Attfield, *J. Chem. Soc., Chem. Commun.* 1185 (1994).
24. M. James and J. P. Attfield, *Chem. Mater.* **7,** 2338 (1995).
25. M. Pechini, U.S. Patent 3,330,697 (1967).
26. A. Manthiram, J. S. Swinnea, Z. T. Sui, H. Steinfing, and J. B. Goodenough, *J. Am. Chem. Soc.* **109,** 6667 (1987).
27. T. Ami, M. K. Crawford, D. C. Johnson, Q. Huang, and R. W. Eewin, *Phys. Rev. B* **51,** 5994 (1995).
28. H. Muller-Buscbaum, *Angew. Chem.* **16,** 674 (1977).
29. J. B. Goodenough and A. Manthiram, *J. Solid State Chem.* **88,** 115 (1990).
30. S. Rakshit and P. S. Gopalakrishnan, *J. Solid State Chem.* **110,** 28 (1994).